Pion-nucleon partial-wave analysis to 2 GeV

Richard A. Arndt, Zhujun Li, L. David Roper, and Ron L. Workman
Department of Physics, Virginia Polytechnic Institute and State University, Blacksburg, Virginia 24061

John M. Ford
MS-50, Teledyne-Brown Engineering, Cummings Research Park, 300 Sparkman Drive, Huntsville, Alabama 35807
(Received 10 August 1990)

We have analyzed the available pion-nucleon elastic-scattering data with laboratory kinetic energies below 2 GeV. We present the results of several energy-dependent and energy-independent analyses performed over this energy range. Pole positions and the corresponding residues are reported for resonances. We compare our results to those from our previous analyses and to values reported by the Particle Data Group.

I. INTRODUCTION

We have analyzed elastic pion-nucleon scattering data up to a laboratory kinetic energy of 2 GeV. This analysis supersedes our last reported analysis[1] to 1.1 GeV. Not only has the energy range been expanded; in addition, much new and precise data have been added at lower energies. The data base is described in Sec. II. As in the previous analysis[1] of Arndt, Ford, and Roper (AFR), we have obtained both energy-dependent and energy-independent solutions. The methods used in obtaining the solutions are discussed in Sec. III. Conventions and constraints applied in the analyses are briefly summarized in Sec. IV. Graphical depictions of our resulting solutions are displayed in Sec. V. Pole positions have been extracted along with their corresponding residues. These results are displayed in Sec. VI. Here our results are compared to those results extracted from the Karlsruhe-Helsinki[2] (KH) and Carnegie-Mellon–Berkeley[3] (CMB) analyses and compiled by the Particle Data Group.[4] We also make comparisons with AFR and point out differences between our resonance spectrum and those of previous analyses.[2–4] Suggestions are made for future experiments.

II. PION-NUCLEON DATA BASE

The data base used in this analysis is considerably different from that used by AFR. Apart from a doubling of the laboratory kinetic energy of data included[5] in our analysis, much new precise data have been added at lower energies.[6] This addition of precise low-energy data has aided in a recent determination[7] of the πNN coupling constant. In addition to cross-section and polarization measurements, a number[8] of R and A data now also exist. In Fig. 1 we display the polarization data to a laboratory kinetic energy of 600 MeV. While data are obviously scarce for the charge-exchange reaction, the lack of forward-angle data in the other channels should also be noted. This lack of data is reflected in the precision with which the spin-flip amplitude can be determined at small angles.

Various aspects of the elastic-scattering data base are summarized in Table I, which shows total data by charge channel for the full energy range (0–2.1 GeV), and for the range (0–1100 MeV); the latter is then compared to the numbers of data used in the AFR analysis. Table I also contains a summary of data below 600 MeV; it is broken into pre-1984 and post-1983 segments to display the large increase in high-quality data coming from "pion factories" in recent years. Rather little data[9] have been added in the 1100–2100 MeV range since 1980.

In the summer of 1987 the low-energy (below 800 MeV) data were "flagged" to reflect the relative quality of various data sets; we were assisted in this effort by Nefkens of UCLA. Each experiments was given a rating of 1*, 2*, or 3* which indicated the relative merit of that measurement. This enabled analyses in which, for example, only higher-quality data could be employed. Generally, a lower rating was assigned to older (superseded) data which played a small role in constraining the fits. Although Table I shows the (0–1100 MeV) data base in present use to contain roughly the same number of data as used in the FA84 analysis,[1] many of the FA84 data

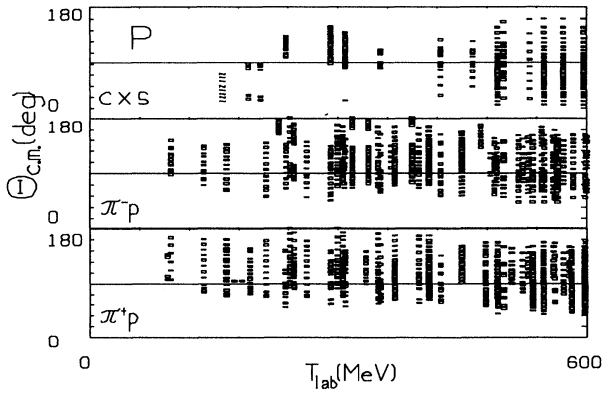

FIG. 1. Pion-nucleon polarization (P) data base to 600 MeV, for $\pi^{\pm}p$ and charge-exchange (CXS) scattering.

TABLE I. Pion-nucleon data base listed by reaction type.

Data limits (MeV)	$\pi^+p\to\pi^+p$	$\pi^-p\to\pi^-p$	$\pi^-p\to\pi^0n$
0–600 Post-83	370	376	197
0–600 Pre-84	1167	1266	512
0–1100 AFR	3711	4942	717
0–1100 Present	4281	5089	1236
1100–2100 Present	5750	4255	896
0–2100 Total	10031	9344	2132

were subsequently flagged 1* and were not included in the present analyses. Not all experiments were rated. Table I includes unflagged experiments as well as 2* and 3* data. Data above 1200 MeV were not flagged so critically as were the lower-energy data, but experiments which extended downward into the lower-energy regime were assigned the same flag rating as was assigned at lower energies. We feel that such a flagging system should be repeated for the entire data base through a collaboration of experimentalists and analysts.

In addition to "flagging," a number of experiments and individual data points are "scratched" from analyses. Scratched data result from conflicts in the data base and also include all polarization data with errors exceeding 0.2 (we consider these data as irrelevant to the fit). Although only those data used in the analyses are shown in Table I, all data are retained in the Scattering Analysis Interactive Dial-in (SAID) system at VPI and SU. Comparisons of any components of the data base are available through the SAID system.

III. ENERGY-DEPENDENT AND ENERGY-INDEPENDENT SOLUTIONS

The energy dependence for global fits was obtained by the coupled-channel Chew-Mandelstam K-matrix representation described by AFR. This produces an elastic-scattering amplitude for each partial wave T_e which can be expressed in terms of a K function $\bar{K}$ as

$$T_e=R_e\bar{K}/(1-C_e\bar{K}) , \tag{1}$$

with

$$\bar{K}=K_e+C_iK_0^2/(1-C_iK_i) . \tag{2}$$

C_e and C_i are the Chew-Mandelstam elastic (πN) and inelastic ($\pi\Delta$) functions described by AFR; R_e, the elastic phase-space factor, is the imaginary part of C_e. In order to control the behavior near the elastic threshold, the K-matrix elements (K_e, K_0, and K_i) were expanded as polynomials in the energy variable $Z=(W_{\text{c.m.}}-W_{\text{th}})/1000$, where $W_{\text{c.m.}}$ and W_{th} are, respectively, the center-of-mass and threshold energies. Multiplying K_0 by an added factor of Z allowed the fixing of scattering lengths by fixing the value of the leading term in K_e. It should be noted that the above $\pi\Delta$ channel is a "generic" inelastic channel. As in the AFR analysis, the S_{11} amplitude was given an additional ηN coupling. Charge splitting was accomplished as in the AFR analysis through multiplication of $\bar{K}$ by an appropriate Coulomb barrier factor.

Single-energy analyses were parametrized as

$$S_e=(1+2iT_e)=\cos(\rho)\exp(2i\delta) . \tag{3}$$

The phase parameters δ and ρ were then expanded as linear functions around the analysis energy, with a slope (energy derivative) fixed from the energy-dependent solution.

Forty-five single-energy solutions were obtained, as described by AFR, by binning the data within some range of energies, obtaining δ and ρ and their energy derivatives at some central energy from the energy-dependent solution, and then determining which phases (δ and ρ) were to be searched. The selection of search parameters was done by an algorithm which found all partial waves with total cross sections in excess of some minimum (determining which δ's were to be fitted) and reaction cross sections exceeding the same minimum (determining which ρ's were to be fitted). Once a δ or ρ was selected for fitting, it was then automatically included at all higher energies. Partial waves not adjusted were thereby fixed at the energy-dependent values. The number of varied parameters ranged from 4 to 30 MeV to 48 at 2050 MeV. Results of the single-energy fits are summarized in Table II and illustrated in a number of partial-wave plots shown in this article.

In practice, the energy-dependent representation was derived through successive iterations with the single-energy fits. Sufficient numbers of parameters were added to accommodate any structures suggested by the, presumably form-independent, single-energy fits. In this fashion, we attempted to eliminate much of the form dependence implicit in the energy-dependent fit.

IV. CONVENTIONS AND CONSTRAINTS

One difference between the analysis presented here and our previous solutions is the adoption of the exact Coulomb rotations used in the Karlsruhe analyses and

described in the *Handbook of Pion-Nucleon Scattering.*[2] The AFR analyses used the same direct Coulomb amplitudes as used by Karlsruhe, but took the Coulomb rotations (multiplying each term of the partial-wave sum) from a point-charge interaction. In practice, the difference is very slight but most pronounced at the higher energies of this analysis. Charge splitting (going from "hadronic" to "nuclear" partial waves) is still different for the VPI and SU[1] and Karlsruhe solutions.[2,10]

Higher partial waves are poorly determined by data at lower energies, so a system of scattering-length constraints was implemented for all the analyses described here. The scattering lengths obtained by Koch[11] from partial-wave dispersion relations were used by adding to the data base χ^2 penalty terms for each partial wave. S and P waves were allowed to vary around the Koch values weighted with a small error while D and higher waves were rigorously constrained by fitting, and not searching, the leading term in the energy expansion for

TABLE II. Comparison of the χ^2 for our energy-independent solutions vs the corresponding χ^2_{ed} from the SM90 energy-dependent solution. The central energy and width of each bin is listed along with the number of parameters searched.

T_{lab} (range) (MeV)	Data/χ^2 (χ^2_{ed})	Parameters	Data/χ^2 (cumulative)
30 (20–40)	162/324 (453)	4	162/324
50 (35–65)	275/515 (584)	5	437/839
75 (66–87)	125/219 (353)	5	562/1058
100 (88–110)	146/202 (259)	6	708/1260
125 (111–139)	130/289 (317)	6	838/1549
150 (140–160)	45/89 (159)	6	883/1638
175 (161–189)	95/154 (247)	6	978/1792
200 (186–214)	98/149 (278)	6	1076/1941
250 (240–265)	87/157 (262)	6	1163/2098
300 (285–315)	325/566 (713)	9	1488/2664
350 (330–370)	171/421 (536)	10	1659/3085
400 (357–425)	204/508 (696)	10	1863/3593
450 (425–475)	342/916 (1201)	12	2205/4509
500 (485–515)	268/580 (687)	14	2473/5089
550 (535–565)	377/786(1070)	17	2850/5875
600 (585–615)	294/532 (709)	18	3144/6407
650 (635–665)	242/472 (918)	20	3386/6879
700 (685–715)	249/433 (1348)	21	3635/7312
750 (730–770)	504/1057 (1805)	22	4139/8369
800 (785–815)	407/722 (1169)	24	4546/9091
850 (830–870)	519/1325 (2003)	27	5065/10 416
900 (880–920)	982/1817 (2887)	31	6047/12 233
950 (925–975)	789/1369 (2171)	34	6836/13 602
999 (975–1025)	774/1315 (1919)	35	7610/14 917
1050 (1025–1075)	641/1187 (1684)	38	8251/16 104
1100 (1075–1125)	783/1490 (2093)	39	9034/17 594
1150 (1125–1175)	666/1143 (1687)	40	9700/18 737
1200 (1175–1225)	698/1607 (2498)	40	10 398/20 344
1250 (1225–1275)	678/1198 (1664)	40	11 076/21 542
1300 (1275–1325)	719/1324 (1897)	40	11 795/22 866
1350 (1325–1375)	713/1439 (1929)	40	12 508/24 305
1400 (1375–1425)	541/903 (1309)	40	13 049/25 208
1450 (1425–1475)	797/1320 (1784)	42	13 846/26 528
1500 (1475–1525)	196/300 (700)	44	14 042/26 828
1550 (1525–1575)	595/1050 (1451)	44	14 637/27 878
1600 (1575–1625)	357/456 (648)	44	14 994/28 334
1650 (1625–1675)	750/1234 (1994)	44	15 744/29 568
1700 (1675–1725)	254/321 (446)	44	15 998/29 889
1750 (1725–1775)	726/1392 (1670)	44	16 724/31 281
1800 (1775–1825)	230/526 (729)	46	16 954/31 807
1850 (1825–1875)	800/1418 (2495)	46	17 754/33 225
1900 (1875–1925)	293/663 (1036)	46	18 047/33 888
1950 (1925–1975)	759/1560 (2383)	48	18 806/35 448
2000 (1975–2025)	237/352 (741)	48	19 043/35 800
2050 (2025–2075)	453/818 (1558)	48	19 496/36 618

TABLE III. Comparison of the χ^2 per datum from our various solutions for the π^+p, π^-p, and charge-exchange (CXS) processes. The number of parameters searched in the isospin $\frac{1}{2}$ and $\frac{3}{2}$ states listed along with the number of constraints imposed on the scattering lengths (SL) and partial waves (PW) and resulting χ^2 for each solution.

Solution	SM90	KV90	CV90	FA84
χ^2/datum (π^+p)	24 897/10 031	26 250/10 031	27 555/10 031	7416/3771
χ^2/datum (π^-p)	24 293/9344	24 957/9344	26 246/9344	10 658/4942
χ^2/datum (CXS)	10 814/2132	9368/2132	9694/2132	2062/717
Parameters ($I=1/2,3/2$)	(76,68)	(88,73)	(89,74)	(64,57)
χ^2/constraints (SL)	142/14	147/14	60/14	
χ^2/constraints (PW)		2695/899	4724/1263	

K_e to the Koch scattering lengths. The χ^2 penalty incurred by these constraints is largely spread throughout the data below 100 MeV, where the data base contains some strongly conflicting measurements.[12] An assessment of the effect of these constraints on the solutions described in this article, particularly the low energies, is ongoing. Any low-energy extrapolation of these solutions (e.g., to the Cheng-Dashen point) would necessarily be tempered by the scattering-length constraints.

We denote as SM90 the energy-dependent solution which we have found in applying the above methods and constraints. Two other energy-dependent solutions were obtained by constraining our solutions to follow the trends of the KH and CMB analyses. These solutions we have denoted as KV90 and CV90, respectively. In addition to the scattering-length constraints mentioned above, these solutions have the KH and CMB partial waves as soft constraints.

In Table III, we compare SM90, KV90, CV90, and our previous solution FA84. Of the two solutions with constrained parial waves, KV90 is the more successful in fitting the data. Both KV90 and CV90 have more structure than SM90 as is evident in the larger number of parameters required to obtain these solutions.

V. PARTIAL-WAVE AMPLITUDES AND OBSERVABLES

Having described our formalism we now display some results of our analyses. Figure 2 shows the quality of our SM90 fit to the total-cross-section data. These data are quite precise and all three of our models show a similar fit. Differences are more evident in predictions for the polarization (P). In Fig. 3 we see that our three models are fairly consistent in their predictions for P in $\pi^{\pm}p$, large deviations coming mainly at the high end of our energy range. Significant differences are visible, however, in the charge-exchange reaction for which data constraints

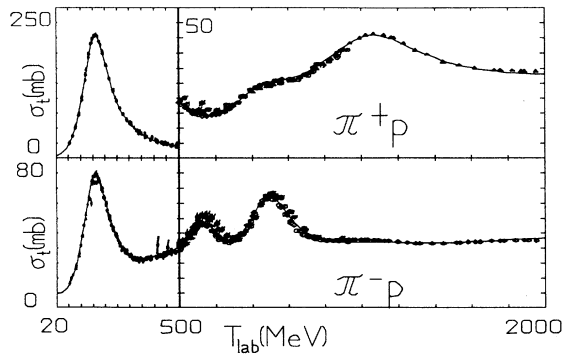

FIG. 2. Total cross sections for $\pi^{\pm}p$ scattering to 2 GeV.

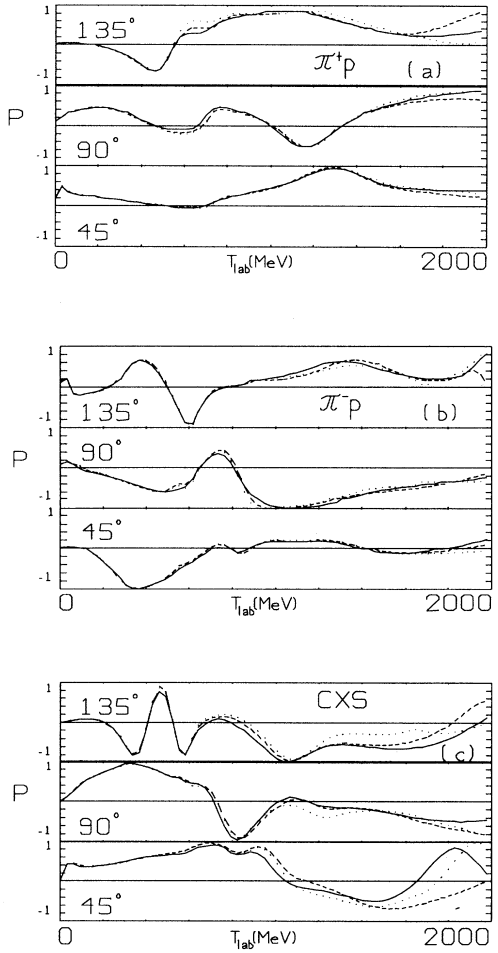

FIG. 3. Polarization (P) predictions for SM90 (solid), KV90 (dashed), and CV90 (dotted) at 45°, 90°, and 135° for (a) π^+p, (b) π^-p, and (c) charge-exchange scattering.

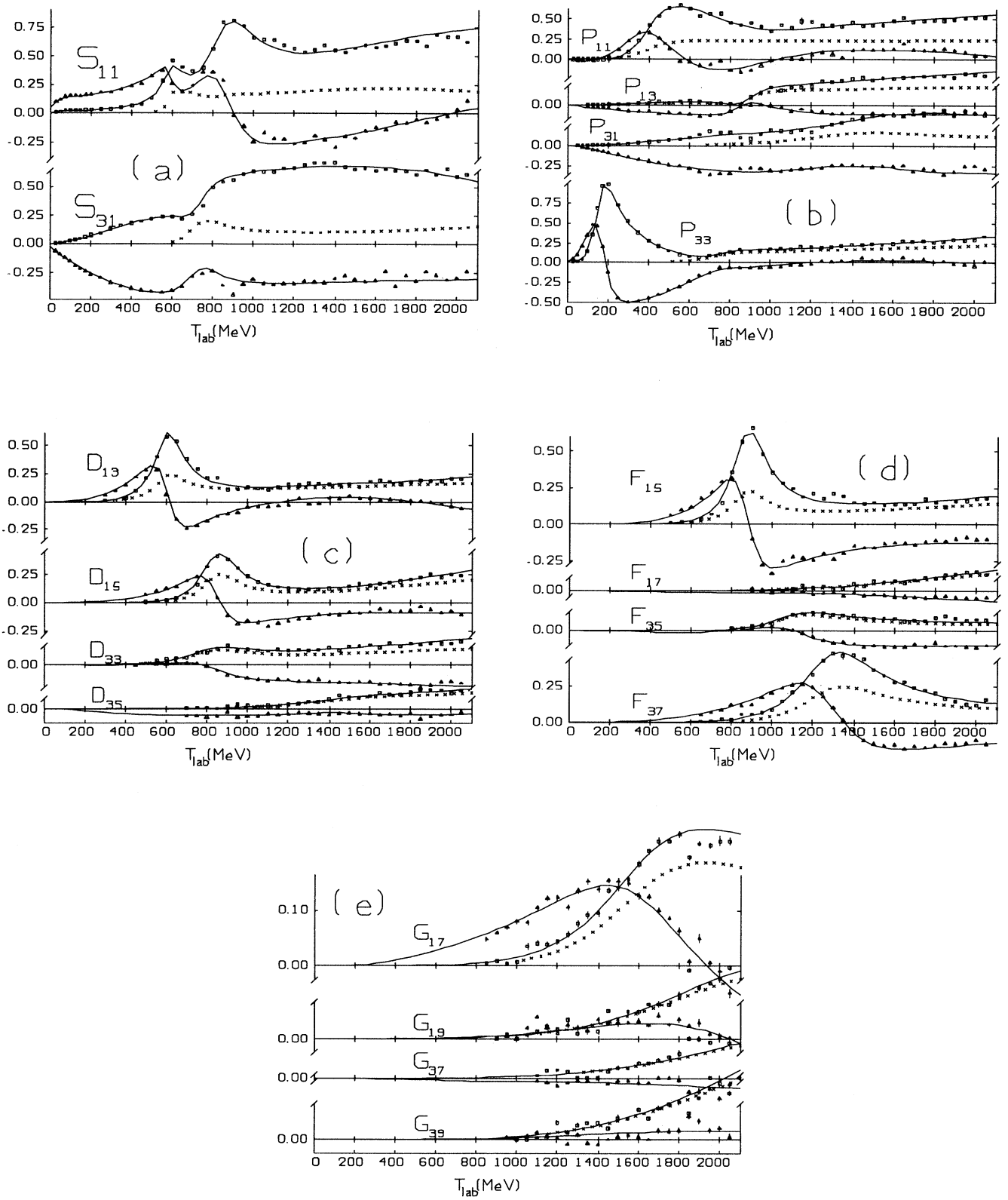

FIG. 4. Partial-wave amplitudes ($L_{2I,2J}$) from the solution SM90. The real part of the energy-independent solution for the T matrix is represented by squares, the imaginary part by triangles, and ($\mathrm{Im}T - T^*T$) is indicated by $\times$. Plotted are the (a) S waves, (b) P waves, (c) D waves, (d) F waves, and (e) G waves.

are much weaker. A primary component of the charge-exchange data base is the polarization data set of Brown.[13] These data, which were treated specially by both the KH and CMB analyses, were included, as published, in these analyses. None of the solutions could be said to fit these data well and, in fact, a large part of the charge-exchange χ^2 for any solution comes from this experiment. We have chosen to include it, however, since it is such a large part of the charge-exchange data base and since very bad fits are concentrated at a few energies only. A complete comparison can be obtained through the SAID system.

Figure 4 shows the partial-wave amplitudes resulting from our solution SM90. Included are the *S*, *P*, *D*, *F*, and *G* partial waves. Resonance behavior is clearly evident in most partial waves, as is the η cusp in S_{11}. We also confirm resonance behavior in an *H* waves, as we shall point out in the next section. Another way to view the resonance structure in this system is to plot the partial-wave contributions to the total cross section. This is done in Fig. 5 for the isospin $\frac{1}{2}$ and $\frac{3}{2}$ waves.

The partial-wave amplitudes of the other solutions, KV90 and CV90, show more similarities than differences when compared with SM90. In Fig. 6 we see that, while the three solutions show qualitative agreement in D_{13} and F_{15}, there are larger differences for the P_{11} partial wave.

In the following section we will present our extracted pole positions and residues for the three solutions. There good agreement will also be seen in the extracted poles and residues for the above F_{15} waves. Poorer agreement will be found for the ever controversial P_{11}.

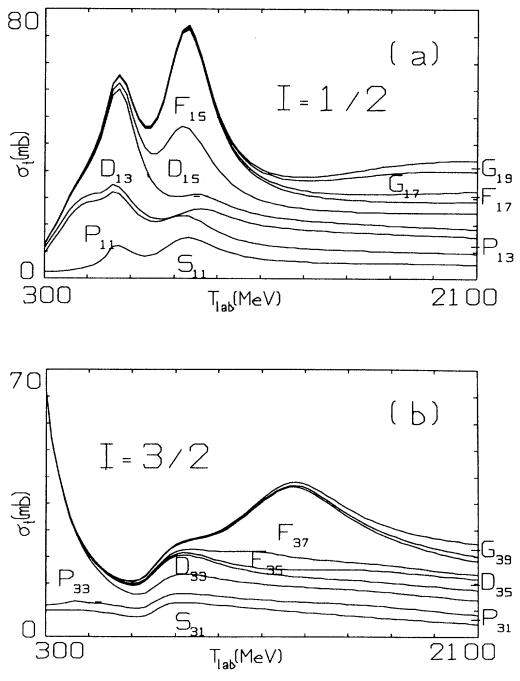

FIG. 5. Contributions to the total cross section from individual partial waves. Contributions from the (a) isospin $\frac{1}{2}$ waves and the (b) isospin $\frac{3}{2}$ waves.

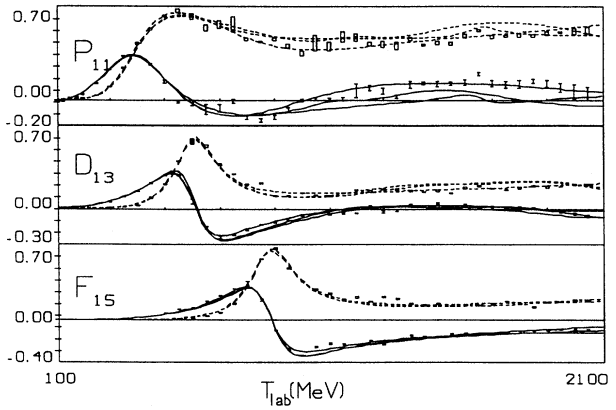

FIG. 6. Comparison of the P_{11}, D_{13}, and F_{15} partial-wave predictions from SM90, KV90, and CV90. The real (imaginary) part of the energy-independent solution is given as boxes (bars). Figures denote the consistency of the three solutions for the D_{13} and F_{15} partial waves and the variation in the P_{11} partial wave.

VI. RESULTS AND DISCUSSION

As was done by AFR, we have searched for poles and zeros in the partial waves we have extracted. The prominent poles and residues for our three solutions are listed in Tables IV and V along with their corresponding Particle Data Group descriptions. As noted in Sec. III, the $\pi\Delta$ channel is used to account for inelasticity in our analyses (ηN being added to the S_{11} channel). The $\pi\Delta$ cut requires that we search a second sheet of the complex plane for poles. The existence of second-sheet poles has a strong influence on only the P_{11} partial wave. This partial wave is illustrated in Fig. 7 where a second-sheet pole is found below the $\pi\Delta$ cut. The interference of this pole with the nearby first-sheet pole and, at a slightly higher energy, a pole-zero pair, produces a complicated structure. Cutkosky and Wang have recently[14] examined this wave. In their analysis a ρN coupling was added and poles were found for both the $P_{11}(1440)$ and $P_{11}(1710)$ on the four resulting sheets. Here the ηN coupling was also found to be large.[14]

In comparing with AFR we find few significant changes in the resonance parameters of any four-star resonances.[4] An exception is the $S_{11}(1535)$. The real part of this resonance pole has increased by 40 MeV. The $P_{13}(1720)$ has moved (lower) by 30 MeV in the SM90 solution and is now consistent with other Particle Data Group values.[4] The imaginary part of the $D_{33}(1700)$ pole position has dropped by a third and is now consistent with the Cutkosky[3,4] value.

Our most interesting results pertain to the three-star and lower rated resonances. In particular we see convincing evidence for a P_{33} resonance near 1600 MeV. We have labeled this resonance the $P_{33}(1600)$, corresponding to a two-star resonance listed by the Particle Data Group.[4] As is displayed in Fig. 8, this resonance is associated with a pole-zero combination in the complex plane. In our previous analysis[1] we claimed to find no evidence for the three-star $P_{11}(1710)$. In Table IV, we see

some evidence for this resonance; however, its existence is still uncertain. If it does exist, however, it must be much broader than was earlier claimed.[3,4] We had also previously[1] claimed to see some evidence for the $D_{13}(1700)$. Its effect was quite weak due to the close association of a pole-zero combination. We no longer feel there is sufficient evidence for its existence. The solutions KV90 and CV90 give evidence for the $S_{31}(1900)$—SM90 does not. Only weak evidence exists for the $P_{33}(1920)$.

In addition to those resonances mentioned above and/or reported previously,[1] we also confirm the existence of the $G_{17}(2190)$, $G_{19}(2250)$, and $H_{19}(2220)$. Two isospin $\frac{3}{2}$ resonances have also been added: the $P_{31}(1910)$ and $D_{35}(1930)$. It is interesting to note that the resonance parameters given by CV90 for the $D_{35}(1930)$ tend to be in better agreement with the original Cutkosky results.[3] The SM90 and KV90 results favor an increased mass and width.

As is evident in Tables IV and V, all three solutions find those resonances given a four-star rating by the Particle Data Group.[4] Differences come in the three-star and lower resonances, with more structure being evident in KV90 and CV90. Unambiguous assignments of some poles to corresponding Particle Data Group resonances were not possible. This is perhaps most obvious for the $P_{11}(2100)$, $D_{13}(2080)$, $D_{35}(1930)$, and $S_{31}(1900)$ resonances. Another P_{11} pole was found in the KV90 solution at $1836-i93$ MeV. In addition, KV90 and CV90 were found to have P_{13} poles at $1863-i154$ MeV and $1834-i148$ MeV, respectively. These poles were not listed in Table IV as they appear to have no corresponding Particle Data Group entry.[4]

TABLE IV. Masses, half-widths ($\Gamma/2$), and elastic half-widths ($\Gamma_{\pi N}/2$) for isospin $\frac{1}{2}$ resonances from the Particle Data Group (Ref. 4) are compared to nearby pole positions from the solutions SM90, KV90, and CV90. The corresponding residues (in brackets) are represented by a modulus and phase (in degrees).

Resonance (* rating)	$\Gamma/2$ (MeV)	$\Gamma_{\pi N}/2$ (MeV)	SM90 (MeV)	KV90 (MeV)	CV90 (MeV)
$S_{11}(1535)$ ****	75	30	$1499-i55$ [23,−13°]	$1509-i43$ [19,8°]	$1507-i39$ [16,9°]
$S_{11}(1650)$ ****	75	45	$1657-i80$ [54,−38°]	$1662-i93$ [65,−32°]	$1659-i104$ [70,−33°]
$P_{11}(1440)$ ****	100	60	$1360-i126$ [109,−93°]	$1364-i117$ [85,−88°]	$1351-i109$ [58,−121°]
					$1476-i165$ [65,42°]
Second sheet			$1413-i128$ [172,−63°]	$1421-i115$ [151,−49°]	$1420-i110$ [140,−46°]
$P_{11}(1710)$ ***	55	10	$1636-i272$ [149,149°]	Not seen	Not seen
$P_{11}(2100)$ *	100	10	Not seen	$1937-i237$ [140,−123°]	$2067-i37$ [3,−16°]
$P_{13}(1720)$ ****	100	15	$1675-i57$ [11,−130°]	$1748-i74$ [9,−26°]	$1745-i71$ [6,−27°]
$D_{13}(1520)$ ****	65	35	$1511-i54$ [33,−10°]	$1509-i60$ [38,−11°]	$1510-i60$ [38,−11°]
$D_{13}(1700)$ ***	100	10	Not seen	Not seen	Not seen
$D_{13}(2080)$ **	100	10	Not seen	$1900-i224$ [63,−41°]	$1926-i239$ [62,−42°]
			Not seen	$2157-i122$ [15,−22°]	$2151-i124$ [13,−29°]
$D_{15}(1675)$ ****	80	30	$1655-i62$ [28,−17°]	$1660-i68$ [29,−10°]	$1660-i68$ [30,−10°]
$F_{15}(1680)$ ****	65	40	$1670-i58$ [37,−14°]	$1675-i55$ [37,−10°]	$1675-i53$ [35,−10°]
$F_{17}(1990)$ **	175	10	Not seen	Not seen	$1941-i253$ [18,−38°]
$G_{17}(2190)$ ****	175	25	$2060-i232$ [54,−44°]	$2092-i263$ [84,−14°]	$2054-i303$ [85,−39°]
$G_{19}(2250)$ ****	150	15	$2243-i325$ [47,−37°]	$2194-i221$ [29,−23°]	$2185-i164$ [18,−14°]
$H_{19}(2250)$ ****	200	35	$2253-i320$ [85,−62°]	$2212-i230$ [58,−24°]	$2232-i260$ [68,−27°]

TABLE V. Parameters for isospin $\frac{3}{2}$ resonances. Notation as in Table II.

Resonance (* rating)	$\Gamma/2$	$\Gamma_{\pi N}/2$ (MeV)	SM90 (MeV)	KV90 (MeV)	CV90 (MeV)
$S_{31}(1620)$	70	20	$1587-i60$	$1615-i47$	$1616-i49$
****			[15,−125°]	[12,−84°]	[12,−87°]
$S_{31}(1900)$	75	10	Not seen	$1743-i93$	$1725-i67$
***				[8,−120°]	[5,−117°]
$P_{31}(1910)$	110	20	$1950-i199$	$1929-i220$	$1901-i152$
****			[37,−91°]	[37,−93°]	[34,−83°]
$P_{33}(1232)$	60	57	$1210-i50$	$1211-i50$	$1211-i50$
****			[52,−31°]	[53,−30°]	[53,−31°]
$P_{33}(1600)$			$1612-i115$	$1625-i115$	$1629-i97$
**			[16,−73°]	[21,−70°]	[17,−60°]
$P_{33}(1920)$	125	20	Not seen	Not seen	$2079-i210$
***					[61,−8°]
$D_{33}(1700)$	125	20	$1646-i104$	$1639-i115$	$1631-i113$
****			[13,−22°]	[15,−26°]	[16,−29°]
$D_{35}(1930)$	125	15	$2018-i199$	$2043-i216$	$1886-i150$
***			[15,−24°]	[40,−35°]	[18,−30°]
$F_{35}(1905)$	150	15	$1794-i115$	$1791-i103$	$1796-i120$
****			[14,−40°]	[13,−36°]	[17,−41°]
$F_{37}(1950)$	120	50	$1884-i119$	$1894-i112$	$1905-i123$
****			[61,−23°]	[59,−13°]	[59,−8°]

In summary, the energy range of our analyses now covers most of the resonances given in the baryon summary table of the Particle Data Group.[4] We have confirmed the presence of all four-star resonances in this energy range. Some surprises have been found in the three-star and lower resonances. Perhaps most interesting is the P_{33} pole found near 1600 MeV. While this resonance is not contained in the baryon summary table it should be noted that a $P_{33}(1690)$ pole is listed in Table 2.4.1.7 of Ref. 15.

The most persistent problem in these analyses is the relatively poor fit to charge-exchange data. As we have shown in Fig. 3, our three models give very different predictions for polarization measurements at the highest energies we have considered. Given that all analyses have difficulty in fitting the polarization data of Brown,[13] an independent and overlapping measurement would be highly desirable. More detailed information, useful in the planning of experiments, can be extracted through the SAID program.

As we have pointed out earlier,[7] tests made to 600 MeV confirm that fixed-t dispersion relations are well satisfied by the solutions presented here. They also result in a πNN coupling constant much lower than that given by Koch and Pietarinen.[16] Given the importance of this issue, updated analysis from the KH and CMB groups would clearly be useful.

While these solutions add a quality of smoothness (S-channel analyticity) to previous analyses, and generally do a better job of fitting data, they may need to be

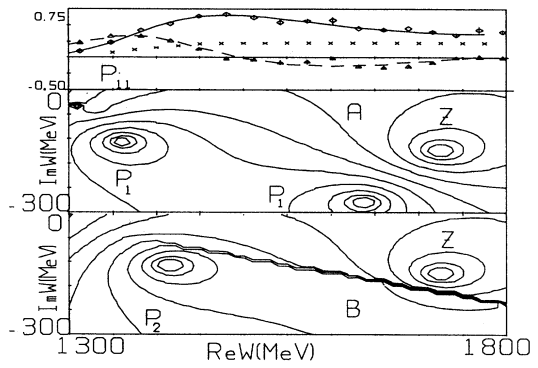

FIG. 7. Amplitude and complex plane plot for the SM90 P_{11} partial wave. Frame A displays the first-sheet poles and zeros. Frame B shows the location of a second-sheet pole below the $\pi\Delta$ cut (visible as a sawtooth line). P_1 (P_2) indicate first- (second-) sheet poles. Z indicates a zero.

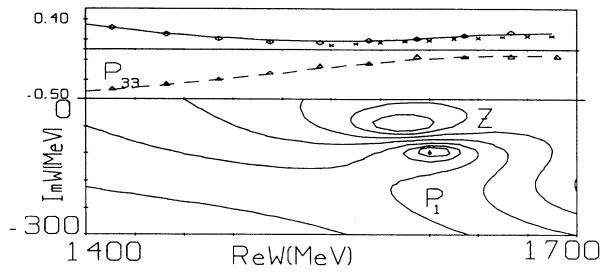

FIG. 8. Amplitude and complex-plane plot for the SM90 P_{33} partial wave. Notation as in Fig. 7.

amended in order to better satisfy some of the two-variable analyticity properties, which the KH and CMB groups have attempted to build into their analyses. Furthermore, the reliability of the energy-dependent fits deteriorates as the upper end of the data base, 2100 MeV, is approached; extrapolation to higher energies is definitely not recommended.

ACKNOWLEDGMENTS

We acknowledge useful communications with R. E. Cutkosky and G. Höhler. This work was supported in part by a U.S. Department of Energy Grant No. DE-AS05-76ER04928.

[1]R. A. Arndt, J. M. Ford, and L. D. Roper, Phys. Rev. D **32**, 1085 (1985).

[2]G. Höhler, F. Kaiser, R. Koch, and E. Pietarinen, *Handbook of Pion-Nucleon Scattering* (Fachsinformationszentrum, Karlsruhe, Germany, 1979), Physics Data 12-1.

[3]R. L. Kelly and R. E. Cutkosky, Phys. Rev. D **20**, 2782 (1979); R. E. Cutkosky *et al.*, *ibid.* **20**, 2804 (1979); **20**, 2839 (1979); in *Baryon 1980,* Proceedings of the IV International Conference on Baryon Resonances, Toronto, Canada, 1980, edited by N. Isgur (University of Toronto, Toronto,1980), p. 19.

[4]Particle Data Group, G. P. Yost *et al.*, Phys. Lett. B **204**, 1 (1988).

[5]We thank R. E. Cutkosky and G. Höhler for their help in the construction of our data base.

[6]More complete information is available from the authors or interactively through the SAID program.

[7]R. A. Arndt, Z. Li, L. D. Roper, and R. L. Workman, Phys. Rev. Lett. **65**, 157 (1990).

[8]D. B. Barlow *et al.*, Phys. Rev. Lett. **62**, 1009 (1989); V. V. Abaev *et al.*, Yad. Fiz. **48**, 1338 (1988) [Sov. J. Nucl. Phys. **48**, 852 (1988)]; M. E. Sadler (private communication).

[9]D. J. Candlin *et al.*, Nucl. Phys. **A364**, 23 (1981); I. G. Alekseev *et al.*, Institute of Theoretical and Experimental Physics, Moscow, Reports Nos. 111-89 (unpublished) and 184-88 (unpublished).

[10]B. Tromborg, S. Waldenstrøm, and I. Øverbø, Phys. Rev. D **15**, 725 (1977).

[11]R. Koch, Z. Phys. C **29**, 597 (1985).

[12]See W. Kluge and G. Smith, in *Proceedings of the Third International Symposium on Pion-Nucleon and Nucleon-Nucleon Physics,* Gatchina, USSR, 1989, edited by I. V. Lopatin and N. C. Morosova (Academy of Sciences of the USSR, Leningrad, 1989); E. Friedman *et al.*, Nucl. Phys. **A514**, 601 (1990); J. T. Brack *et al.*, Phys. Rev. C **41**, 2202 (1990).

[13]R. M. Brown *et al.*, Nucl. Phys. **B144**, 287 (1978).

[14]R. E. Cutkosky and S. Wang, Phys. Rev. D **42**, 235 (1990).

[15]G. Höhler, in *Pion-Nucleon Scattering,* edited by H. Schopper, Landolt-Börnstein, New Series, Group 1, Vol. 9, Pt. b (Springer, New York, 1983).

[16]R. Koch and E. Pietarinen, Nucl. Phys. **A336**, 331 (1980).